Experimental Study of Endwall Heat Transfer in a Linear Cascade

(article starts on next page)

Experimental Study of Endwall Heat Transfer in a Linear Cascade

To cite this article: Lei Wang *et al* 2012 *J. Phys.: Conf. Ser.* **395** 012028

View the article online for updates and enhancements.

Experimental Study of Endwall Heat Transfer in a Linear Cascade

Lei Wang[1], Bengt Sundén[1], Valery Chernoray[2], Hans Abrahamsson[3]

[1] Department of Energy sciences, Lund University, Lund 22100, Sweden
[2] Thermal and Fluid Dynamics, Chalmers University of Technology, Gothenburg, 41296, Sweden
[3] Volvo Aero Corporation, Trollhättan, 46181, Sweden

Corresponding author's e-mail: lei.wang@energy.lth.se

Abstract. The endwall heat transfer characteristics of forced flow past outlet guide vanes (OGVs) in a linear cascade have been investigated by using a liquid crystal thermography (LCT) method. Due to the special design of an OGV profile, the focus of this study is emphasized on the heat transfer patterns around the leading part of a vane. The Reynolds number is kept constant at 260,000. Two attack angles of the vane are considered. For $\alpha = 0°$, the vane obstructs the incident flow like a bluff body and a remarkable flow separation phenomenon was noticed. For $\alpha = 30°$, the vane is more "streamlined" with respect to the incoming flow and no obvious flow separation was observed. In general, the endwall heat transfer for $\alpha = 0°$ is higher than that for $\alpha = 30°$.

1. Introduction

Low pressure turbine outlet guide vanes (OGVs) are positioned in the last vane row in a turbine rear frame. The OGVs have both an aerodynamic and a structural function. In structural terms they compose a frame which provides a structural connection between the aft bearing support, the main engine carcass, and the aircraft attachment point. In aerodynamic terms they form the last part of the engine internal path before the nozzle. The efficiency of the low pressure turbine has a significant effect on the overall specific fuel consumption. A 1% increase in low pressure turbine efficiency gives rise to 0.7% increase in overall engine efficiency [1]. Therefore, increasing the engine efficiency requires knowledge of the aerodynamic and heat transfer performance of the OGVs.

The main aerodynamic function of OGVs is to de-swirl the flow coming from the last low pressure turbine rotor into an axial outflow. The flow around an OGV includes boundary layer development, secondary flows as well as the risk of separation both on the vane itself and on the end walls (central hub and the outer shroud). In modern gas turbines, the endwall regions become more and more thermally loaded. This requires that the endwall heat transfer be carefully considered in turbine designs, especially in the vicinity of the blade and downstream. Extensive investigations have been made on endwall heat transfer of turbine blades [2-8]. In this study, we carried out heat transfer measurements on the endwall of OGVs in a large-scale linear cascade. The attack angle of the OGVs with respect to the mainstream is 0° and 30°, respectively. The Reynolds number is kept at 260,000. Liquid crystal thermography (LCT) was used to measure the surface temperature and map the local

heat transfer distribution on the endwall. One of the objectives of this study is to validate CFD methods for optimizing OGV design.

2. Experimental Setup

Experiments were performed in a cascade facility located in Chalmers University of Technology. The facility is a low-speed blow-down linear cascade consisting of a wide angle diffuser (area ratio between the diffuser outlet and inlet is 4), a settling chamber, a three dimensional contraction chamber (contraction ratio is 5), an inlet-section and a test section with boundary-layer suction, see Fig. 1. The test section is designed out of two pairs of parallel discs where the inner discs constitute the upper and lower end-walls of OGV's, as shown in Fig. 2. The cross section of the working area of the facility is 200 by 1200 mm and the OGV cascade has 7 vanes. The flow is driven by a 30 kW centrifugal fan and passes through a wide-angle diffuser, a settling chamber, and a contraction. The level of the incoming flow turbulence intensity was adjusted by a turbulence grid which was placed 700 mm upstream of the cascade. The OGV consists of a 2D profile section which is extended in the span direction. The vane axial chord is 220 mm and the span is 200 mm. An OGV profile includes four sections, i.e., the leading edge, the trailing edge, a two-part suction side, and the pressure side, as shown in Fig. 3. The leading and the trailing edges are described by an ellipse and a circular arc, respectively. The pressure side is designed as an elliptic curve matching the leading and trailing edges. The suction side is created in two parts, firstly an arc which matches the leading edge and continues to the maximum thickness and from there an ellipse, which matches the curvature of the arc. The elliptic region ranges from the maximum thickness to the trailing edge on the suction side. Cascade vanes are manufactured using a stereo-lithography technique, which has a typical accuracy of ±0.1% of the model size. More details concerning the design of the linear cascade can be found in [9].
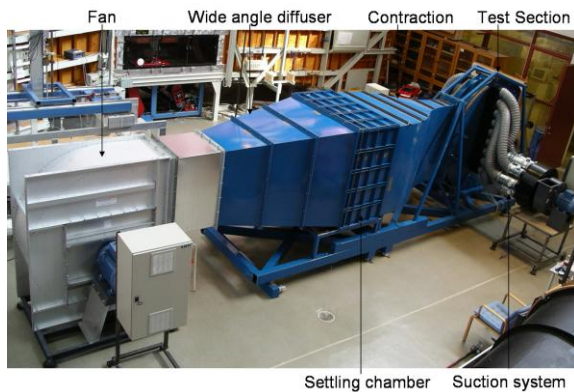

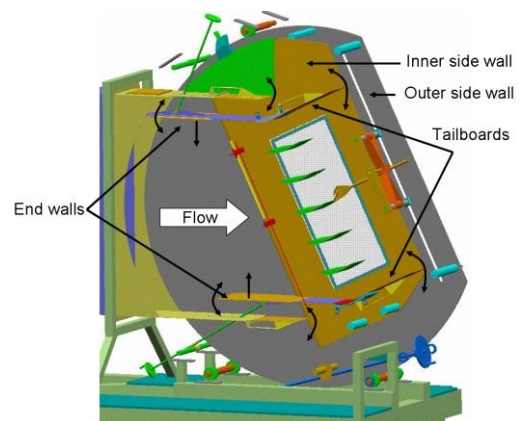Fig. 1   The test facility.

Fig.2   The test section for heat transfer measurement.

Heat transfer measurements were performed on an endwall which is made of Plexiglass to provide an optical path for a CCD camera. The thickness of the endwall is 20 mm and the thermal conductivity of the material is 0.2 W/mK. Part of the endwall is covered by a heating foil and is referred to as the heat transfer target wall. The size of the heater is 500 by 320 mm. The heater is made of an etched constantan foil due to its low temperature coefficient of resistance. Figure 4 shows the heating foil pattern. The width of wire is 1.87 mm and the gap between two neighboring wires is 0.27 mm. Due to the gaps between the wires, the heat flux across the span of the heater is not perfectly uniform (the non-uniformity is estimated to be less than 5%). The surface temperature is measured by an LCT sheet which is the same size as the heater. In this study, the LCT sheet, R35C5W (manufactured by LCR Hallcrest Ltd), is used to measure the surface temperature and obtain the heat transfer coefficients.

Before the experiments, the LCT sheet was calibrated to obtain the relationship between the temperature and the hue. LCT images were captured by a GigE Vision CCD camera which allows 1600 by 1200 pixel resolution. In this study, the spatial resolution of the LCT images is 0.22 mm/pixel. During the experiment, the CCD camera, illumination lighting, and the test section were covered by a dark enclosure to prevent interference from the surrounding light noise.
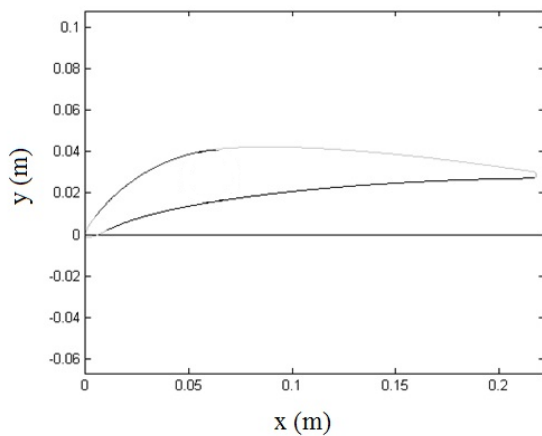

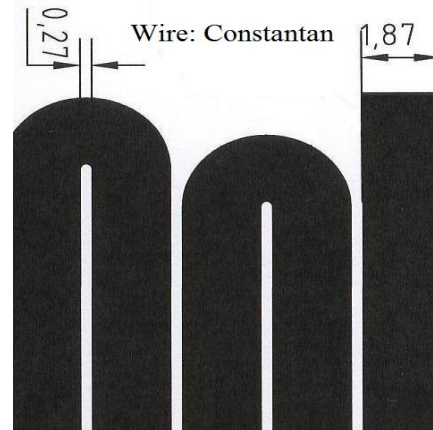Fig. 3 The final design of an OGV profile.

Fig.4   Heating foil pattern.

3. Data Reduction

The Reynolds number is defined as

$$\mathrm{Re} = U_0 L/\nu \tag{1}$$

where U_0 is the free-stream bulk velocity, and L is the vane axial chord length. In this study, the Reynolds number is kept constant at 260,000.

The heat transfer coefficient h, is calculated based on the Newton's law of cooling, i.e.,

$$h = \dot{q}_w/(T_w - T_{in}) \tag{2}$$

where $\dot{q}_w$ is the wall heat flux, and T_w and T_{in} are, respectively, the wall temperature and the inlet air temperature. When calculating the heat flux $\dot{q}_w$, the radiative and conductive heat losses are estimated. Using a diffuse gray-surface model in which the emissivity is 0.8, it is found that the radiative heat loss is less than 5%. The heat conduction loss is quite low and is negligible. The heat transfer coefficient h is obtained is such a manner. After steady state is achieved, a number of LCT images are generated, each corresponding to a distinct wall heat flux. In interpreting the temperature, the green colour is chosen as the reference colour because it is the most temperature-sensitive colour in the calibration curve. The green colour is characterized by hue values ranging from 60 to 100. By proper adjustment of the wall heat flux, the reference colour is moved from one location to another such that the entire area of interest is eventually covered with the reference colour. Thereby the heat transfer coefficient over the entire area can be obtained. More details of the LCT technique for obtaining the heat transfer coefficients over an entire area can be found in [10-12].

The heat transfer coefficient is represented in terms of Nusselt number Nu, which is defined as $\mathrm{Nu} = hL/k$, where k is the thermal conductivity of air. Uncertainty analysis is performed by applying the method proposed by Moffat [13]. The uncertainty in the local heat transfer coefficients is estimated to be within 10% based on the 95% confidence level. This value takes into account the effects of the

measuring errors in voltage, current, LCT reading, non-uniformity of the heat flux, and the heat losses to the surroundings.

4. Preliminary Test

Prior to experiments, LCT was calibrated to obtain the relationship between temperature and hue. The LCT sheet was applied on the surface of an aluminium plate towards which a CCD camera was directed. On the other side of the plate, six thermocouples were fitted to measure the temperature. The accuracy of the thermocouple is 0.03 °C. The calibration was performed in a wooden black box in which the aluminium plate was placed. The air is heated by a heater which is connected with a fan. The air temperature can be adjusted by controlling the power of the heater. It was found that the non-uniformity of temperature across the aluminium plate is less than 0.1 °C. At a thermal equilibrium state, the LCT image was captured by a CCD camera and the temperature was recorded by a data logger. Thus a calibration curve could be established. More details of the calibration process can be found in, e.g., [14]. Figure 5 shows the calibrated hue-temperature profile, in which the three basic colours, i.e., red, green, and blue corresponds to different hue value ranges. Because the green is the most temperature-sensitive colour, this colour is selected as a reference colour. In the present study, the green colour is characterized by hue values ranging from 60 to 100. Figure 6 shows the LCT images of green colour, in which the hue value varies from 64 to 99, corresponding to the temperature change from about 36.6 °C to 40 °C. Based on this calibration profile, the LCT can be applied to the real heat transfer measurements provided that the optical arrangement, such as the illuminating light, the lighting/viewing characteristics, the camera system, etc., is kept the same.
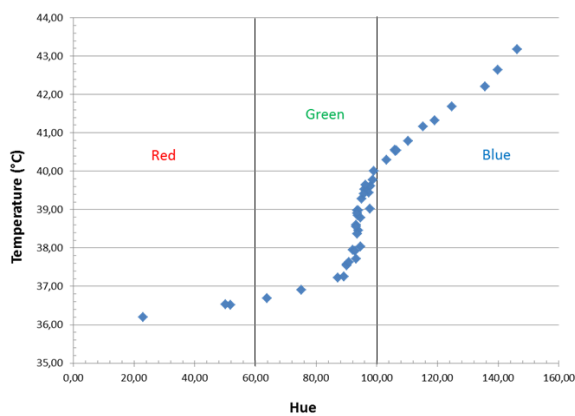

Fig. 5 Calibration profile of LCT.

Fig. 6 Correspondence between hue values and temperature in green colour.

5. Results

In the present study, it is of interest to know the endwall heat transfer in the region around the leading part of the OGV vane. Figure 7 shows the Nusselt number contours on the endwall as the angle of attack is 0 degree ($\alpha = 0°$). In this figure, a Cartesian coordinate system is employed in which x-axis is the streamwise direction, and z-axis is the spanwise direction. All the distances are normalized by the vane chord length L. The origin is placed at the leading edge of the vane. But it should be pointed out that the leading edge of the OGV on the heat-transfer plate is not exactly coincident with the other one projected on the opposite wall due to the parallax error in the CCD camera.

For α = 0°, the incident flow is parallel to the direction of the vane axial chord. However, due to the broad flattened front of the vane, the object acts more like a bluff body with respect to the incoming flow. The maximum heat transfer occurs in the vicinity of the leading edge where the flow separates and is deflected downstream. A shear layer is found at the at the pressure side (concave side) of the vane which is characterized by a relatively high Nusselt number region. The heat transfer is enhanced in such a manner that the formed horseshoe vortices entrain the cooler fluid in the mainstream to the endwall. Further inspection of Fig. 7 shows that the separated shear layer does no reattach on the pressure side until $x/L = 0.55$. In the corner region between the pressure side and the shear layer, the heat transfer coefficient experiences a drop in magnitude. This might be attributed to the fact that an elongated separation bubble is formed in between and the fluid flow is nearly stagnant compared to the mainstream. At the suction side (convex side), the shear layer is much thinner and it attaches on the vane throughout the considered region. The shear layer represents a relatively high heat transfer region, but it decays quickly in the spanwise direction as the distance moves away from the suction side of the vane.
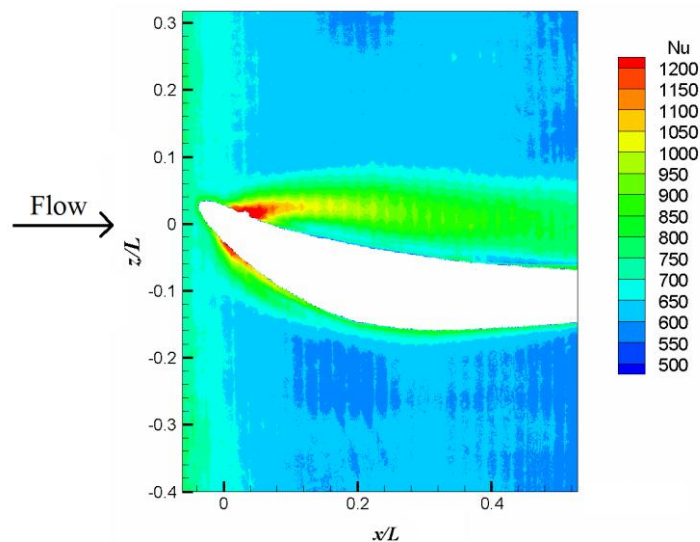

Fig. 7   Endwall Nusselt contours at α = 0° for Re = 260,000.

Figure 8 shows the endwall Nusselt number contours at α = 30° for Re = 260,000. In this case, the vane is inclined with respect to the incoming flow. However, due to the special design of the profile, the vane, to a large extent, looks like a "streamlined" object. The flow is split into two parts by the leading edge of the vane and there are no noticeable separated shear layers as observed in Fig. 7. In addition, it is found that the endwall heat transfer is higher in the leading part of the vane. But with the growth of the boundary layer, the heat transfer decays gradually in the streamwise direction.

Figure 9 shows the profiles of spanwise-averaged Nusselt number $\overline{\mathrm{Nu}}$ for the different attack angles. The spanwise-averaged Nusselt number is calculated in the measured region, i.e.,

$$\overline{\mathrm{Nu}}(x/L) = \int_{z/L=-0.46}^{z/L=0.26} \mathrm{Nu}(x/L, z/L) \, d(z/L) \tag{3}$$

It is noted that both profiles in Fig. 9 demonstrate the small-scale oscillating behaviour, which can be attributed to the non-uniformity of the heat flux across the heating foil. For $x/L > 0$, the $\overline{\mathrm{Nu}}$ profile for

$\alpha = 0°$ is higher than that at $\alpha = 30°$, indicating that the attack angle has a significant effect on heat transfer. Further inspection of Fig. 9 reveals that the $\overline{\text{Nu}}$ profile for $\alpha = 30°$ drops more quickly in the streamwise direction. For $\alpha = 0°$, however, the $\overline{\text{Nu}}$ profile decreases in a moderate manner. Also included in Fig. 9 is the Nusselt number for a flat-plate boundary layer, i.e., $\text{Nu}_x = 0.0296\text{Re}_x^{0.8}\,\text{Pr}^{1/3}$ [15]. For the sake of convenient comparison, Re_x is simply taken as 260,000. It is found that the endwall of OGVs has higher Nusselt number than the flat-plate boundary layer.
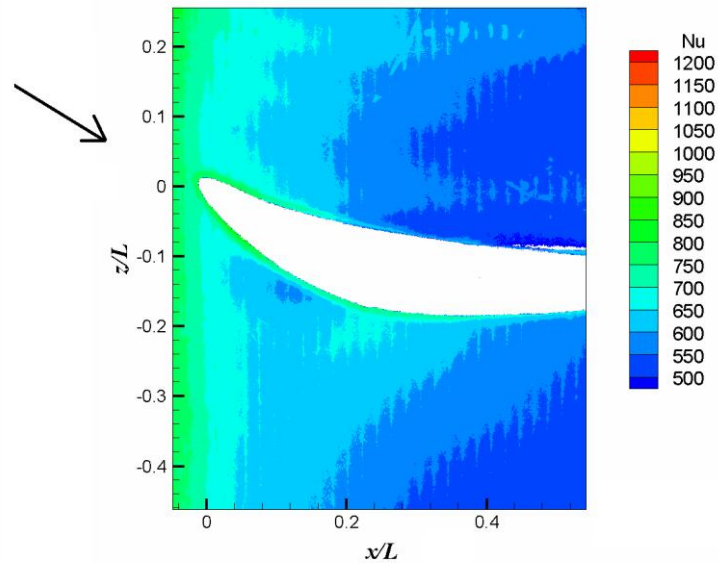

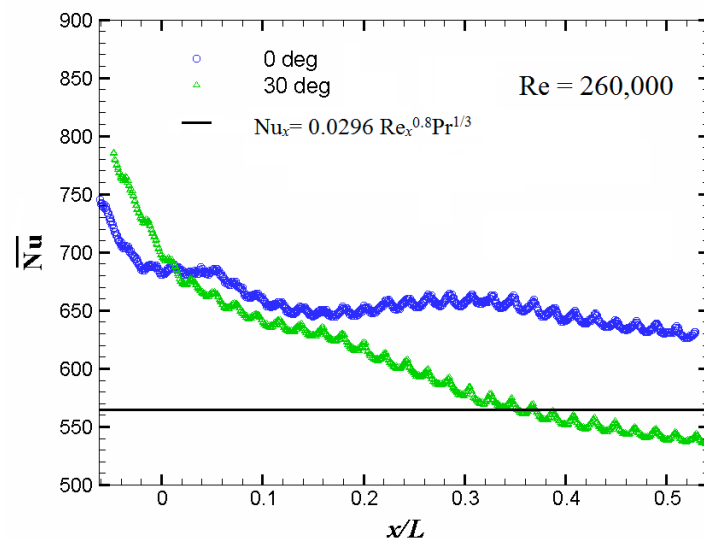Fig. 8   Endwall Nusselt number contours at $\alpha = 30°$ for Re = 260,000.

Fig. 9   Spanwise-averaged Nusselt number distribution along the endwall.

6. Summary

In the present study, liquid crystal measurements were carried out to investigate the endwall heat transfer of an OGV in a linear cascade. The Reynolds number is kept constant at 260,000. Two attack angles of the vane were considered. For $\alpha = 0°$, the vane acts more like a bluff body with respect to the incoming flow. Due to the broad flattened front of the vane, remarkable flow separation phenomenon was noticed. For $\alpha = 30°$, on the contrary, the vane acts more like a streamline object with respect to the incident flow. No obvious flow separation was observed. In general, the heat transfer is higher for $\alpha = 0°$, indicating that the attack angle of the vane has a significant effect on the endwall heat transfer.

7. Acknowledgement

References

[1]   Wisler, D.C., 1998, The technical and economical relevance of understanding blade row interaction effects in turbomachinary, in *Blade row interference effects in axial turbomachinery stages*, Von Karman Institute for Fluid Dynamics, LS 1998-02.

[2]   Graziani, R.A., Blair, M.F., Taylor, J.R., and Mayle, R.E., 1980, An experimental study of endwall and airfoil surface heat transfer in a large scale turbine blade cascade, *J. Engineering for Power*, **102**, 257-267.

[3]   Goldstein, R.J., and Spores, R.A., 1988, Turbulent transport on the endwall in the region between adjacent turbine blades, *ASME J. Heat Transfer*, **110**, 862-869.

[4]   Wang, H.P., Olson, S.J., Goldstein, R.J., and Eckert, E.R.G., 1997, Flow visualization in a linear turbine cascade of high performance turbine blades, *ASME J. Turbomach.* **119**, 1-8.

[5]   Han, S., and Goldstein, R.J., 2006, Influence of blade leading edge geometry on turbine endwall heat (mass) transfer, *ASME J. Turbomach.* **128**, 798-813.

[6]   Han, S., and Goldstein, R.J., 2007, Heat transfer study in a linear turbine cascade using a thermal boundary layer measurement technique, *ASME J. Heat Transfer*, **129**, 1384-1394.

[7]   Lorenz, M., Stripf, M., Schulz, A., and Bauer, H.J., 2008, External heat transfer measurements on a turbine airfoil in a linear cascade, *In proceedings 19th International Symposium on Transport Phenomena*, Reykjavik. Iceland.

[8]   Han, S., and Goldstein, R.J., 2008, The heat/mass transfer analogy for a simulated turbine endwall, *Int. J. Heat Mass Transfer*, **51**, 3227-3244.

[9]   Hjärne, J., 2007, Turbine outlet guide vane flows, PhD thesis, Chalmers University of Technology, Göteborg, Sweden.

[10]   Wang, L., Sundén, B., Borg, A., and Abrahamsson, H., 2011, Heat transfer characteristics of an impinging jet in crossflow, *ASME J. Heat Transfer*, **133**, 122202.

[11]   Wang, L., Sundén, B., Borg, A., and Abrahamsson, H., 2011, Control of jet impingement heat transfer in crossflow by using a rib, Int. J. Heat Mass Transfer, **54**, 4157-4166.

[12]   Wang, L., Salewski, M., Sundén, B., Borg, A., and Abrahamsson, H., 2012, Endwall convective heat transfer for bluff bodies, *Int. J. Commu. Heat Mass Transfer*, **39**, 167-173.

[13]   Moffat, R.J., 1998, Describing the uncertainties in experimental results, *Exp. Thermal and Fluid Sciences*, **1**, 3-17.

[14]   Gao, X. and Sundén B.,, 2000, Detailed measurements of heat transfer coefficients in a rectangular duct using hue-based calibration liquid crystal, *Int. Commu. Heat Mass Transfer*, **1**, 13-22.

[15]   J.H. Lienhard IV, and J.H. Lienhard V, *A Heat Transfer Textbook*, 2008, Phlogiston Press.